

Surface topology, electrophysical properties and formation mechanism of tin(ii) sulfide thin films

N. S. Kozhevnikova^{1,a}, L. N. Maskaeva^{2,b}, A. N. Enyashin^{1,c}, A. P. Tyutyunnik^{1,d},
O. A. Lipina^{1,e}, I. O. Selyanin^{1,f}, V. F. Markov^{2,g}

¹Institute of Solid State Chemistry of the Ural Branch of RAS, Ekaterinburg, Russia

²Ural Federal University, Ekaterinburg, Russia

^akozhevnikova@ihim.uran.ru, ^blarisamaskaeva@yandex.ru, ^cenyashin@ihim.uran.ru, ^dtyutyunnik@ihim.uran.ru,
^elipinaolgaa@yandex.ru, ^fsioprostreet@mail.ru, ^gv.f.markov@urfu.ru

Corresponding author: N. S. Kozhevnikova, kozhevnikova@ihim.uran.ru

PACS 81.10.Dn, 82.60.Lf, 82.70.Dd, 81.05.Hd

ABSTRACT Photosensitive nanocrystalline SnS films with a size of coherent X-ray scattering regions of about 30 nm were obtained by chemical bath deposition. It has been demonstrated that the deposition time affects significantly both microstructure and thickness of the film as well as the size of the particles' agglomerates forming the film. The current sensitivity of the obtained films was studied. All synthesized films, regardless of the duration of synthesis, reveal *p*-type conductivity due to Sn vacancies. Atomic force microscopy measurements and fractal approach provide a detailed description of the processes occurring during film formation. The characteristics of the fabricated SnS films are potentially useful for design of advanced absorbing layers within thin film solar cells.

KEYWORDS tin(II) sulfide, thin films, chemical bath deposition, *p*-type conductivity, quantum-chemical calculations, formation mechanism

ACKNOWLEDGEMENTS This work was carried out in accordance with the scientific and research plans and state assignment of the ISSC UB RAS and Ural Federal University Program of Development within the Priority-2030 Program (Ministry of Science and Higher Education of the Russian Federation).

FOR CITATION Kozhevnikova N.S., Maskaeva L.N., Enyashin A.N., Tyutyunnik A.P., Lipina O.A., Selyanin I.O., Markov V.F. Surface topology, electrophysical properties and formation mechanism of tin(ii) sulfide thin films. *Nanosystems: Phys. Chem. Math.*, 2023, **14** (6), 699–704.

1. Introduction

Tin (II) sulfide (SnS) belongs to the family of binary semiconductor chalcogenides and occurs in nature in the form of mineral Herzenbergite. The crystal lattice of SnS consists of layers with a strong covalent intralayer Sn-S bonding and with a weak van der Waals interlayer interaction [1]. Effective technology for creating thin film solar cells requires semiconductor materials satisfying certain criteria. The chemical elements comprising a material must be relatively nontoxic, earth abundant and cheap. For high efficiency of solar energy conversion, the material of absorbing layer should have optimal value of optical band gap E_g , high optical absorption coefficient α , high quantum yield of excited charge carriers, large diffusion length of charge carriers and low recombination rate. SnS possesses a direct E_g of 1.2–1.5 eV, indirect E_g of 1.1 eV, large $\alpha > 10^4 - 10^5 \text{ cm}^{-1}$, and high free carrier concentration around $10^{17} - 10^{18} \text{ cm}^{-3}$, hence, representing a promising material for the absorbing layer of new generation thin film solar cells [1–4].

In this paper, thin SnS films are synthesized by chemical bath deposition from aqueous solutions. The effect of deposition time on the microstructure of the resulting nanocrystalline films is demonstrated, the conductivity type and current sensitivity have been studied. Based on the atomic force microscopy data, a mechanism for the formation of a SnS film on a dielectric substrate is proposed. To substantiate the stoichiometry of chemical composition the quantum chemical calculations have been carried out.

2. Experimental

SnS films were obtained by chemical bath deposition from aqueous solutions using tin chloride SnCl_2 , sodium thio-sulfate $\text{Na}_2\text{S}_2\text{O}_3$ and sodium citrate $\text{Na}_3\text{C}_6\text{H}_5\text{O}_7$ (Na_3Cit). Deposition was carried out in a LOIP LT–112a thermostat at 343 K with an accuracy of $\pm 0.5^\circ$ in maintaining temperature. SnS films were deposited on sital substrates during 30, 60, 90 and 120 minutes. The reaction baths contained 0.06 M SnCl_2 , 0.15 M Na_3Cit and 0.06 M $\text{Na}_2\text{S}_2\text{O}_3$. The pH value was maintained in the range from 2.5 to 3.0.

TABLE 1. Characteristics of SnS thin films chemically deposited on sitall substrates from SnCl₂ and Na₂S₂O₃ aqueous solutions at 343 K

| Synthesis time, min | Unit cell parameters | | | Average film thickness, nm | E_g , eV | j , nA/cm ² at 10 V | | |
|---------------------|----------------------|------------|------------|----------------------------|------------|----------------------------------|------------|----------------------|
| | a , Å | b , Å | c , Å | | | j_{light} | j_{dark} | j_{light}/j_{dark} |
| 60 | 11.318(5) | 3.9963(11) | 4.2865(22) | 210 | 0.94 | 58.83 | 32.90 | 1.79 |
| 90 | 11.3003(3) | 3.9963(7) | 4.2775(15) | 480 | 1.01 | 139.60 | 88.15 | 1.58 |
| 120 | 11.282(4) | 3.9957(6) | 4.2807(15) | 670 | 1.12 | 147.16 | 78.38 | 1.89 |

The crystal structure and phase composition of the films were studied using the X-ray diffractometer Stadi-P (Stoe) in the Bragg-Brentano geometry with CuK_α radiation in the angle range $2\theta = 5 - 100^\circ$ with a step of $\Delta(2\theta)^\circ = 0.03^\circ$ and 70 second exposure. The thickness of the films was determined using the Linnik MII-4M microinterferometer. The light transmission spectra were recorded using a UV-3600 spectrophotometer (Shimadzu, Japan) in the wavelength range of 200–1700 nm with a scanning step of 1 nm.

The morphological characteristics and elemental composition of the films were studied by scanning electron microscopy (SEM) on the TESCAN MIRA 3 LMU electron microscope (TESCAN, Czech Republic). The topology and surface roughness were studied by semi-contact atomic force microscopy (AFM) on the NT-MDT NTEGRA Prima II complex. A silicon cantilever with resonant frequency of 230 kHz and a radius of curvature of the probe less than 10 nm was used to scan the surface. To analyse the surface topology of the films, areas of SnS films with a size of $5 \times 5 \mu\text{m}^2$ were selected and captured from the total surface area of the sample. The AFM images were processed by the Gwyddion program.

The type of SnS films conductivity was determined by the thermal probe method. To register the sign of the thermoelectric force, the digital multimeter DT-830 B was used. The volt-ampere characteristics of the films were measured in both the dark room and as illuminated by a light beam from the solar radiation simulator Zolix GLORIA-X500A, equipped with an Osram XBO 500W/H OFR lamp, under standard conditions: AM1.5G spectrum, illumination 100 mW/cm², temperature 298 K. The magnitude of the current was recorded by the Keithley 2450 source measure unit.

The density-functional theory (DFT) calculations within periodic boundary conditions were performed using the SIESTA 4.0 package [5]. Generalized Gradient Approximation (GGA) with the Perdew-Burke-Ernzerhof (PBE) parametrization was employed for description of exchange-correlation potential. The core electrons were treated within the frozen core approximation, applying norm-conserving Troullier-Martins pseudopotentials. The double- ζ polarized basis set (DZP) was used for description of the valence orbitals of all elements.

3. Results and discussion

The X-ray diffraction spectra of SnS films revealed a set of reflexes typical for α -SnS (sp. gr. *Pnma*). The unit cell parameters with corresponding standard quadratic deviations are given in Table 1. The experimental error is determined to be several times greater than indicated in parentheses, since the diffraction patterns of SnS overlap with patterns from several phases composing sitall substrate as well as due to the SnS peaks widening. The X-ray phase analysis did not reveal any tin-containing crystalline phase except α -SnS. The determination of the exact sizes of the coherent scattering regions (CSR) by the Williamson-Hall extrapolation method is rather evaluative due to the broadening anisotropy of the diffraction reflexes. The CSR average value is 26 nm for all synthesized films, which indicates the growth termination of the SnS single crystallites after 60 min of synthesis.

According to energy dispersive X-ray spectroscopic analysis (EDX), the elemental composition of the synthesized SnS films corresponds to the average contents of Sn and S as 40.3 and 41.1 at.%. The content of O is 18.6 at.% and it is due to surface oxygen. The etching of films with an argon beam allows to clean the surface of samples and get rid of oxygen almost completely (for example, down to ~ 1 at.% after etching the film with an Ar⁺ beam to a depth of 6 nm).

According to SEM data, at the initial stage of synthesis (up to 30 min) the grain-like SnS particles of 300–400 nm in length and 50–100 nm in diameter are formed (Fig. 1a). These particles agglomerate into an insular film with a large number of voids and depressions. After 60 minutes, the number of loose large agglomerates with a Feret diameter of ~ 1 microns, consisting of particles 200–300 nm in length and 50–100 nm in diameter (Fig. 1b), increases. Taking into account the average film thickness of ≈ 210 nm after 60 min (Table 1), these agglomerates should have a flat-like organization and cover the substrate in two-dimensional space. After 90 min of deposition, the film thickens, i.e. the individual large agglomerates are no longer visible, and the film becomes a structure formed from small elongated particles of ~ 80 –200 nm (Fig. 1c). At the end of synthesis (after 120 min), the SnS film completely covers the substrate and consists mainly of particles with linear sizes of 80–200 nm (Fig. 1d).

TABLE 2. Surface roughness parameters and fractal dimension of SnS films obtained by processing of AFM images with a surface area of $5 \times 5 \mu\text{m}^2$

| Microrelief parameter | | Deposition time, min | | | |
|--|----------------------|----------------------|-------|-------|-------|
| | | 30 | 60 | 90 | 120 |
| Arithmetic mean roughness R_a , nm | | 158.0 | 75.4 | 112.3 | 91.5 |
| Root-mean-square roughness R_q , nm | | 194.4 | 97.2 | 142.6 | 115.1 |
| The coefficient of asymmetry of the roughness profile R_{sk} | | -0.4 | 0.1 | -0.3 | -0.2 |
| Maximum profile height R_z , nm | | 506.5 | 393.3 | 440.3 | 322.0 |
| Fractal dimension D_f of the surface | Cube counting method | 2.35 | 2.31 | 2.35 | 2.38 |
| | Triangulation method | 2.44 | 2.42 | 2.44 | 2.48 |

Thus, with an increase in the synthesis duration, the amount of the SnS solid phase on the substrate increases, the SnS layers become denser, while the shape and size of grain-like SnS particles remain unchanged. The grain-like SnS particles are agglomerates consisting of nanoparticles ~ 26 nm in size.

Fig. 2 shows typical AFM images of SnS films illustrating a significant difference in surface topology. The films are formed from agglomerates, the amount and shape of which depend on the deposition time. This is consistent with the SEM data (Fig. 1).

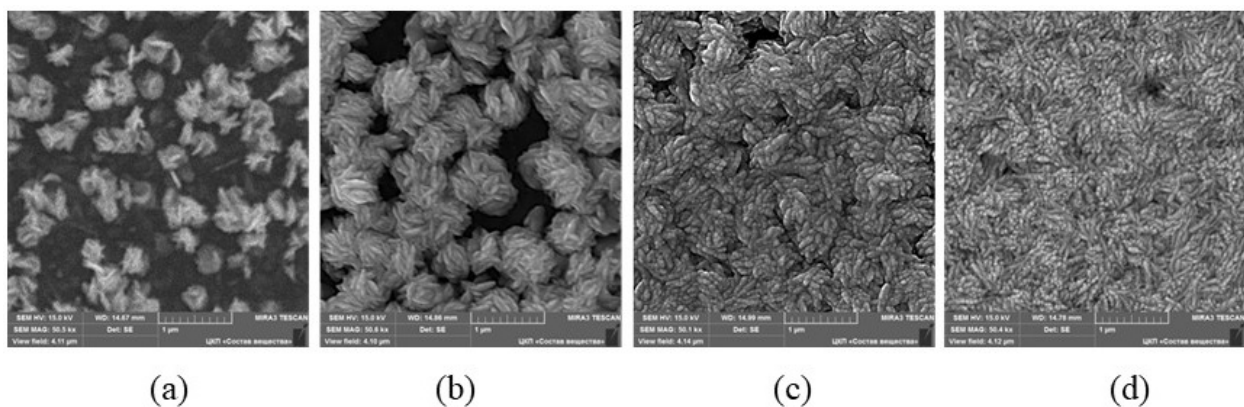


FIG. 1. Morphology evolution of SnS thin films on sital substrate depending on the deposition time, min: a – 30; b – 60; c – 90; d – 120

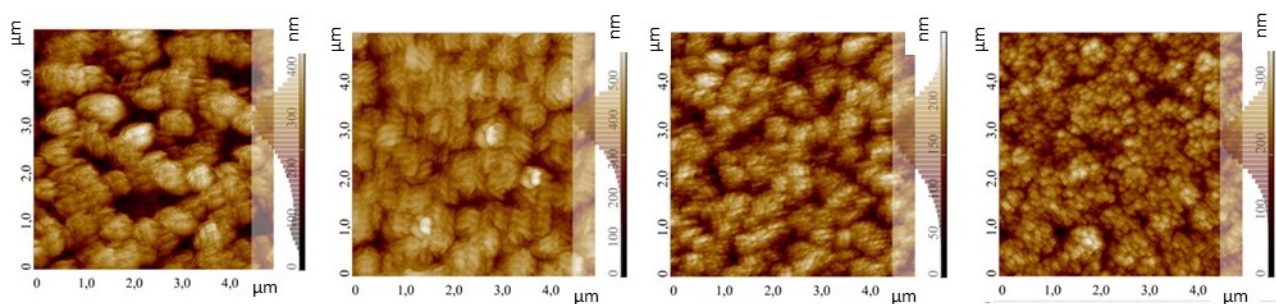
FIG. 2. Surface topology of the SnS thin films on sital substrate depending on the deposition time, min: a – 30; b – 60; c – 90; d – 120. The dimension of AFM images is $5 \times 5 \mu\text{m}^2$

Table 2 presents the parameters describing the surface topology of the SnS films at different duration of synthesis. All samples are characterized by a sufficiently bright heterogeneity of the surface relief, as evidenced by the significant difference between the maximum height of the surface profile R_z and the parameters determining the arithmetic mean R_a and the root-mean-square R_q values of roughness.

The surface of the SnS films reveals a colloid microstructure from the first minutes of deposition. The colloidal particles are represented as the large agglomerates of nanoparticles (Fig. 1,2). Considering a colloidal particle as a fractal cluster (fractal agglomerate), the fractal geometry methods can be applied to describe the thin film microstructure [6–16]. Any fractal cluster as a geometric system is formed as a result of the association (adhesion) of solid particles, and the conditions of association affect the way of cluster growth [12]. The SEM and AFM data (Fig. 2,3) reveal the SnS fractal clusters look like disordered systems, but they may possess an internal order. The parameter characterizing this order numerically is the surface fractal dimension D_f [12]. The D_f values for SnS films are obtained by the processing of AFM images and are tabulated (Table 2). According to [8,9,11,12], the obtained D_f values indicate that the formation of fractal clusters of SnS occurs in three-dimensional space, i.e. mainly within the solution volume according to the “cluster-particle” Witten-Sander model. The role of the free primary particles is performed by SnS nanoparticles.

At the first stage of film deposition, the formation of SnS nanoparticles takes place within the solution bulk. This process obeys the classical crystallization model: a fixed number of crystalline SnS nuclei arises in the supersaturated solution at the initial moment, then SnS nuclei grow to nanoparticles about 26 nm during the first 30 min. At the second stage, the grain-like clusters are formed as a result of collision and agglomeration of these nanoparticles. In the Witten-Sander model, the associating nanoparticles perform Brownian motion in the solution before collision resulting in a cluster. At the third stage, grain-like clusters are deposited on the substrate with film formation (Fig. 1,2). It should be noted that the processes of secondary nucleation due to high supersaturation is quite likely to take place in the solution. After 120 min of deposition, the grain-like clusters/agglomerates are arranged densely on the substrate (Fig. 2d), which excludes the possibility of linear motion trajectories or multiple collisions before sticking and reveals the kinetically controlled agglomeration [10]. This confirms the implementation of the Witten-Sander model. An invariability of D_f (Table 2) indicates that, regardless of the duration of deposition, the mechanism of film formation is preserved [15] and the film surface remains self-similar (self-affine [16]). Thus, the fractal approach provides a deeper understanding of the processes occurring during the formation of SnS thin film on a substrate [15].

The calculation of E_g for SnS was carried out for the case of indirect allowed transitions [6]. Extrapolation of the linear part of function $[\alpha h\nu]^{1/2} = C_2(h\nu - E_g)$ on the abscissa axis allowed to determine the E_g value. The E_g for films deposited after 60, 90 and 120 min are found equal to 0.94, 1.01 and 1.12 eV, respectively (Table 1), which is consistent with the previously published values [2–4].

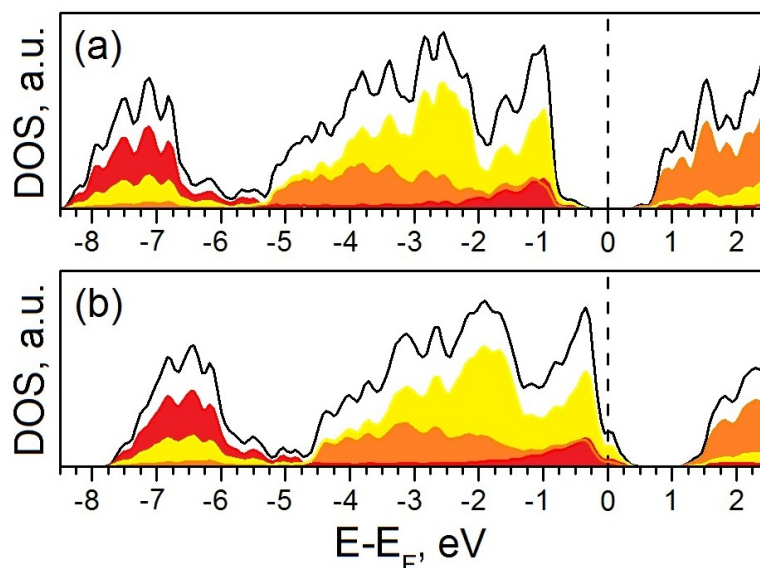


FIG. 3. The total and partial densities of electronic states (DOS) for a (001)SnS slab with perfect stoichiometry (a) or with the Sn atom vacancies in the bulk (b). The Sn5s-, Sn5p- and S3p-states are painted in red, orange and yellow, respectively. DFT GGA calculations

According to the thermo-EMF method, all synthesized SnS films have p -type conductivity. It is known that for binary tin sulfides with only intrinsic lattice defects, the n - or p -type of conductivity is determined by an excess of Sn or S atoms, respectively [7]. In this work, the role of tin vacancies in regulating the type of SnS conductivity is confirmed by DFT calculations of the electronic structure of α -SnS. $3a \times 3b$ supercell of (001)SnS slab of three molecular layers thick was employed as a model of nanoscale SnS. According to the calculations, such a “perfect” film is a semiconductor with the E_g value of at least 1.09 eV (Fig. 3a). The bottom of conduction band is represented by Sn5p-states, while the top of the valence band consists of S3p-states with an admixture of Sn5n and Sn5s-states. These basic features of the SnS electronic structure remain even after introduction of the Sn vacancies, both in the bulk and on the surface. However, the Fermi level

of SnS shifts to the edge of the valence band, which really corresponds to the change from the intrinsic conductivity to the p -type conductivity (Fig. 3b).

The resistivity of the obtained SnS films was studied both under lighting conditions and in the darkness. Fig. 4 shows the volt-ampere $j(U)$ characteristics of SnS thin films in the dark and while illuminated by a light beam of 100 mW/cm^2 at 298 K. A linear course of $j(U)$ curves passing through the origin is observed over the entire area of applied voltages, which indicates the ohmic nature of the obtained SnS films. After illumination of the film surface, the j increased due to the increase in the concentration of free charge carriers. The maximum photocurrent density under illumination $j_{light} = 147.16 \text{ nA/cm}^2$ at 10 V is observed for SnS film obtained after 120 min, and the maximum value of the dark current density $j_{dark} = 88.15 \text{ nA/cm}^2$ is found for SnS film after 90 min of synthesis (Table 1).

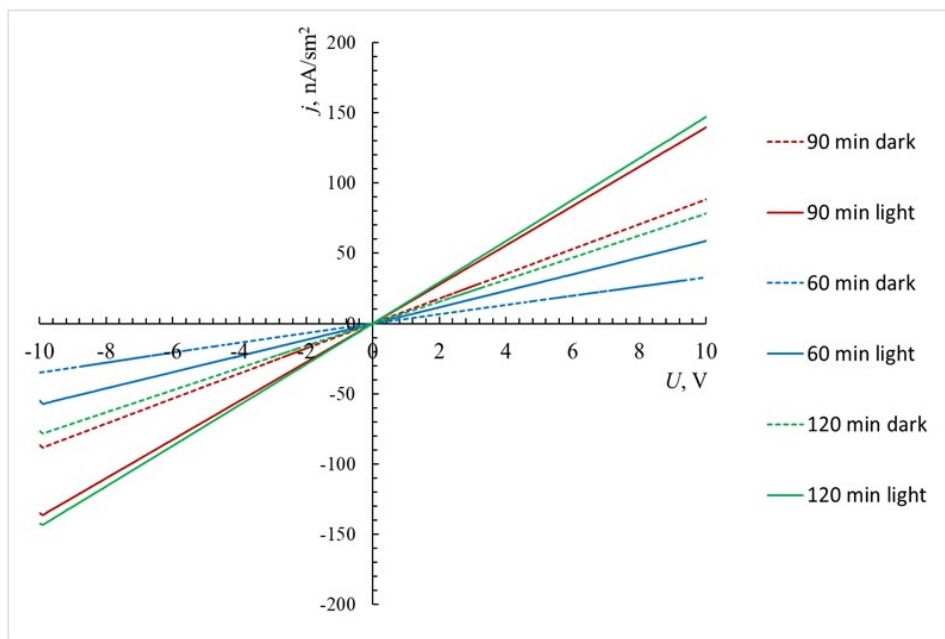


FIG. 4. Current-voltage characteristics of SnS films on siall substrates at different deposition times either in the dark room or under illumination by a light beam of 100 mW/cm^2 (light)

For the film deposited after 30 min, the values of j_{light} and j_{dark} are close to zero (Table 1), which indicates the absence of photosensitive properties. The latter is related to the morphology of SnS (Fig. 1,2): the layer after 30 min is formed from individual agglomerates and has an insular character, strong difference in the profile height ($200 \pm 150 \text{ nm}$) and significant roughness (Table 2). SnS films deposited after 60 and 120 min possess the highest values of the ratio j_{light}/j_{dark} , which are 1.8 and 1.9, respectively (Table 1). At the same time, these films have the lowest values of the arithmetic mean roughness $R_a = 75.4$ and 91.5 nm (Table 2), respectively. The thickness of these films varies in the range from 210 to 670 nm. Thus, the continuity and roughness of the substrate coating do affect primarily the value of j_{light}/j_{dark} , while no noticeable effect of the film thickness on the value of j_{light}/j_{dark} was found. To obtain the photosensitive layers based on SnS, solid films with a minimal roughness and with a thickness of at least 200 nm should be deposited.

4. Conclusion

Thin films of α -SnS were obtained by chemical deposition from aqueous solutions. The effect of the deposition time on their microstructure and their surface topology is presented. The volt-ampere characteristics revealed the optimal film thickness of at least 200 nm for obtaining photosensitive layers. The synthesized films possess a superstoichiometric composition of $S \approx 1 \text{ at.}\%$. Quantum-chemical calculations confirm the role of Sn vacancies as the main progenitors of observed p -type conductivity of SnS films. The formation mechanism of a thin SnS film on a dielectric substrate proceeds according to the “cluster-particle” model, and the formation of initial fractal clusters of SnS occurs in three-dimensional space, i.e. within the solution bulk.

References

- [1] Brent J.R., Lewis D.J., Lorenz T., Lewis E.A., Savjani N., Haigh S.J., Seifert G., Derby B., O'Brien P. Tin(II) Sulfide (SnS) Nanosheets by Liquid-Phase Exfoliation of Herzenbergite: IV-VI Main Group Two-Dimensional Atomic Crystals. *J. Am. Chem. Soc.*, 2015, **137**(39), P. 12689–12696.
- [2] Banai R.E., Horn M.W., Brownson J.R.S. A review of tin(II) monosulfide and its potential as a photovoltaic absorber. *Solar Energy Materials & Solar Cells*, 2016, **150**, P. 112–129.

- [3] Sinsersuksakul P., Heo J., Noh W., Hock A.S., Gordon R.G. Atomic layer deposition of tin monosulfide thin films. *Adv. Energy Mater.*, 2011, **1**, P. 1116–1125.
- [4] Reddy K.T.R., Reddy N.K., Miles R.W. Photovoltaic properties of SnS based solar cells. *Sol. Energy Mater. Sol. Cells*, 2006, (90), P. 3041–3046.
- [5] García A., Papior N., Akhtar A., Artacho E., Blum V., Bosoni E., Brandimarte P., Brandbyge M., Cerdá J.I., Corsetti F., Cuadrado R., Dikan V., Ferrer J., Gale J., García-Fernández P., García-Suárez V.M., García S., Huhs G., Illera S., Korytár R., Koval P., Lebedeva I., Lin L., López-Tarifa P., Mayo S.G., Mohr S., Ordejón P., Postnikov A., Pouillon Y., Pruneda M., Robles R., Sánchez-Portal D., Soler J.M., Ullah R., Yu V.W., Junquera J.J. Siesta: Recent developments and applications. *J. Chem. Phys.*, 2020, **152**, P. 204108.
- [6] Titova L.V., Fregoso B.M., Grimm R.L. Chapter 5: Group-IV monochalcogenides GeS, GeSe, SnS, SnSe, in book Chalcogenide: From 3D to 2D and Beyond. *Woodhead Publishing Series in Electronic and Optical Materials*, 2020, P. 119–151.
- [7] Vidal J., Lany S., d’Avezac M., Zunger A., Zakutaev A., Francis J., Tate J. Band-structure, optical properties, and defect physics of the photovoltaic semiconductor SnS. *Applied Physics Letters*, 2012, **100**(3), P. 032104.
- [8] Roldughin V.I. Fractal structures in disperse systems. *Russian Chemical Reviews*, 2003, **72**(10), P. 823–847.
- [9] Roldughin V.I. The characteristics of fractal disperse systems. *Russian Chemical Reviews*, 2003, **72**(11), P. 913–937.
- [10] Samsonov V.M., Kuznetsova Y.V., D’yakova E.V. Fractal properties of aggregates of metal nanoclusters on solid surface. *Russian Journal of Applied Physics*, 2016, **86**(2), P. 71–77.
- [11] Feder E. *Fractals*. Moscow: Mir, 1991, 260 p. (In Russian).
- [12] Smirnov B.M. *Physics of fractal clusters*. Moscow: Nauka, 1991. 136 p. (In Russian).
- [13] Antonov A.S., Sdobnyakov N.Y., Ivanov D.V., Podbolotov K.B. Morphology investigation study of the copper films relief on a mica surface. *Fiziko-khimicheskie aspekty izucheniya klasterov, nanostruktur i nanomaterialov* [Physical and chemical aspects of the study of clusters, nanostructures and nanomaterials], 2017, **9**, P. 19–26, (In Russian).
- [14] Sdobnyakov N.Y., Antonov A.S., Ivanov D.V. Morphological characteristics and fractal analysis of metal films on dielectric surfaces. Tver: Tver State University, 2019, 168 p. (In Russian).
- [15] Brylkin Y.V., Kustov A.L. Correlation between fractal dimension and different roughness for copper samples. *Fiziko-khimicheskie aspekty izucheniya klasterov, nanostruktur i nanomaterialov* [Physical and chemical aspects of the study of clusters, nanostructures and nanomaterials], 2013, **5**, P. 33–38, (In Russian).
- [16] Panin A.V., Shugurov A.R. Application of fractal description for image analysis in scanning probe microscopy. *Poverkhnost* [Surface], 2003, **6**, P. 62–69, (In Russian).

Submitted 17 October 2023; revised 25 October 2023; accepted 8 November 2023

Information about the authors:

N. S. Kozhevnikova – Institute of Solid State Chemistry of the Ural Branch of RAS, Ekaterinburg, Russia; kozhevnikova@ihim.uran.ru

L. N. Maskaeva – Ural Federal University, Ekaterinburg, Russia; larisamaskaeva@yandex.ru

A. N. Enyashin – Institute of Solid State Chemistry of the Ural Branch of RAS, Ekaterinburg, Russia; enyashin@ihim.uran.ru

A. P. Tyutyunnik – Institute of Solid State Chemistry of the Ural Branch of RAS, Ekaterinburg, Russia; tyutyunnik@ihim.uran.ru

O. A. Lipina – Institute of Solid State Chemistry of the Ural Branch of RAS, Ekaterinburg, Russia; lipinaolgae@yandex.ru

I. O. Selyanin – Institute of Solid State Chemistry of the Ural Branch of RAS, Ekaterinburg, Russia; sioprostreet@mail.ru

V. F. Markov – Ural Federal University, Ekaterinburg, Russia; v.f.markov@urfu.ru

Conflict of interest: the authors declare no conflict of interest.